Noncentrosymmetric superconductor BeAu

A. Amon,[1] E. Svanidze,[1] R. Cardoso-Gil,[1] M. N. Wilson,[2] H. Rosner,[1] M. Bobnar,[1] W. Schnelle,[1] J. W. Lynn,[3] R. Gumeniuk,[4] C. Hennig,[5] G. M. Luke,[2,6] H. Borrmann,[1] A. Leithe-Jasper,[1] and Yu. Grin[1]

[1]*Max-Planck-Institut für Chemische Physik fester Stoffe, Nöthnitzer Straße 40, 01187 Dresden, Germany*
[2]*Department of Physics and Astronomy, McMaster University, Hamilton, ON, Canada L8S4M1*
[3]*NIST Center for Neutron Research, National Institute of Standards and Technology, Gaithersburg, Maryland 20899, USA*
[4]*Technische Universität Bergakademie Freiberg, Institut für Experimentelle Physik, Leipziger Str. 23, 09596 Freiberg, Germany*
[5]*Helmholtz-Zentrum Dresden-Rossendorf, Institute of Resource Ecology, Bautzner Landstr. 400, 01328 Dresden, Germany*
[6]*Canadian Institute for Advanced Research, Toronto, ON, Canada M5G1Z7*

(Received 14 November 2017; revised manuscript received 7 December 2017; published 4 January 2018)

Mixed spin-singlet and spin-triplet pairing can occur in noncentrosymmetric superconductors. In this respect, a comprehensive characterization of the noncentrosymmetric superconductor BeAu was carried out. It was established that BeAu undergoes a structural phase transition from a low-temperature noncentrosymmetric FeSi structure type to a high-temperature centrosymmetric structure in the CsCl type at $T_s = 860$ K. The low-temperature modification exhibits a superconducting transition below $T_c = 3.3$ K. The values of lower ($H_{c1} = 32$ Oe) and upper ($H_{c2} = 335$ Oe) critical fields are rather small, confirming that this type-II ($\kappa_{G\text{-}L} = 2.3$) weakly coupled ($\lambda_{e\text{-}p} = 0.5$, $\Delta C_e/\gamma_n T_c \approx 1.26$) superconductor can be well understood within the Bardeen-Cooper-Schrieffer theory. The muon spin relaxation analysis indicates that the time-reversal symmetry is preserved when the superconducting state is entered, supporting conventional superconductivity in BeAu. From the density functional band structure calculations, a considerable contribution of the Be electrons to the superconducting state was established. On average, a rather small mass renormalization was found, consistent with the experimental data.

DOI: 10.1103/PhysRevB.97.014501

I. INTRODUCTION

Since the discovery of superconductivity over a century ago, much progress has been made in both utilizing and understanding this intriguing phenomenon. Many groups of materials exhibiting superconductivity have been found and studied thoroughly in hopes of establishing a mechanism for electron pairing that would lead to higher critical temperatures and fields. Two symmetries are particularly important for the superconducting state: time-reversal and inversion symmetry [1]. If at least one of them is absent, Cooper pairing will likely appear in an unconventional form. While noncentrosymmetric superconductors (NCSCs) have been known for quite some time, the field received a significant boost when $CePt_3Si$, the first noncentrosymmetric compound in which superconductivity is accompanied by a heavy-fermion behavior, was discovered [2]. The absence of inversion symmetry gives rise to Fermi surface splitting, which in turn promotes both intraband and interband pairing [3]. Consequently, this produces an admixture of spin-singlet and spin-triplet components, with the ratio governed by the strength of the spin-orbit coupling [4,5]. Furthermore, if spin-orbit coupling is strong, topological superconductivity may arise in NCSCs [6–8].

Although time-reversal symmetry (TRS) breaking has been observed in a number of centrosymmetric superconductors [Sr_2RuO_4 ($T_c = 1.5$ K [9,10]), UPt_3 ($T_c = 0.5$ K [11–13]), Th-substituted UBe_{13} ($T_c = 0.9$ K [14]), (Pr; La)(Os; Ru)$_4Sb_{12}$ ($0.74\ \text{K} \leqslant T_c \leqslant 1.85$ K [15–17]), $PrPt_4Ge_{12}$ ($T_c = 7.9$ K [18]), $LaNiGa_2$ ($2.1\ \text{K} \leqslant T_c \leqslant 2.7$ K [19,20]) and $LaNiC_2$ ($T_c = 2.7$ K [20]), $Y_5Rh_6Sn_{18}$ ($T_c = 3$ K [21]), and $Lu_5Rh_6Sn_{18}$ ($T_c = 4$ K [22])], NCSCs are thought to be more likely to break TRS. Nonetheless, while a large number of NCSCs were studied systematically [23–35], TRS breaking has only been confirmed in Re_6Zr ($T_c = 6.75$ K [36,37]), Re_6Hf ($T_c = 5.98$ K [38]), SrPtAs ($T_c = 2.4$ K [39]), and La_7Ir_3 ($T_c = 2.25$ K [40]). Given that TRS breaking has only been established in a handful of materials, comprehensive studies of existing NCSCs are crucial in order to determine the origin of this exotic phenomenon.

The crystal structure of BeAu was previously reported to be noncentrosymmetric with the cubic FeSi structure type in the space group $P2_13$ [$a = 4.659(1)$ Å] [41]. Subsequent works indicate a tetragonally distorted crystal structure along with a possible high-temperature structural phase transition [42,43]. Superconductivity of BeAu was first stated to occur below $T_c = 2.64$ K [44], with another report of $T_c = 3.2$ K [45]. Given conflicting T_c values and material quality issues [42,45], an in-depth analysis of single-phase BeAu is necessary.

In this work, we present physical properties of polycrystalline, single-phase BeAu. It was established that BeAu undergoes a structural phase transition from the low-temperature (LT) FeSi structure type to a high-temperature (HT) CsCl structure type at $T_s = 860$ K. The LT-BeAu exhibits Bardeen-Cooper-Schrieffer (BCS)-type superconductivity below $T_c = 3.3$ K. A full Meissner flux expulsion, along with a resistivity drop below T_c and $\gamma_n \approx \gamma_s$ signal bulk superconductivity. LT-BeAu can be classified as a weakly coupled superconductor with $\Delta C_e/\gamma_n T_c \approx 1.26$, $\lambda_{e\text{-}p} = 0.5$, and $2\Delta(0)/k_B T_c = 3.72$. The lower ($H_{c1} = 32$ Oe) and upper ($H_{c2} = 335$ Oe) critical

 ©2018 American Physical Society

fields provide an estimate for the Ginzburg-Landau parameter of $\kappa = 2.34$ and mean-free path $l/\xi_0 = 1.15$, classifying LT-BeAu as a type-II superconductor in the clean limit.

II. EXPERIMENTAL AND COMPUTATIONAL METHODS

The polycrystalline samples were synthesized by arc melting from elements Be (Heraeus, >99.9 wt.%) and Au (Alfa Aesar, >99.95 wt.%) in a 51:49 ratio, with mass loss of 0.3%. A small excess of beryllium was added in order to compensate for the Be loss due to evaporation. Complete sample preparation was performed in argon-filled glove boxes [MBraun, $p(H_2O/O_2) < 0.1$ ppm], dedicated to the handling of Be-containing samples [46]. The obtained BeAu specimens have a silver metallic luster. The as-cast samples were placed in an alumina crucible, sealed in a tantalum tube, and annealed in a tube furnace (HTM Reetz, Berlin, Germany) at 400 °C for 48 h in inert Ar atmosphere. Both as-cast and annealed samples did not exhibit any air or moisture sensitivity.

Differential thermal analysis (DTA) was performed on a Netzsch DTA 404 PC in the range from 600 to 1100 K, in alumina crucibles under a steady Ar flow with a heating/cooling rate of 10 K min^{-1}.

Synchrotron powder diffraction data were recorded at the Rossendorf Beamline BM20 at the European Synchrotron Radiation Facility (ESRF, Grenoble, France). Sieved powdered samples (grains < 20 μm) were diluted with quartz powder, packed in a quartz capillary (0.3 mm diameter) and measured using a NaI(Tl)-scintillation detector.

Neutron diffraction data were collected on the BT-1 powder diffractometer at the NIST Center for Neutron Research. Collimators of 15′, 20′, and 7′ were used before and after the Cu (311) monochromator and after the sample, respectively, and data were collected in steps of 0.05° in the 2θ range of 20° to 150°. A powder sample of LT-BeAu was packed in a cylindrical vanadium sample container with 6 mm diameter.

The temperature-dependent x-ray powder diffraction (XRPD) pattern was recorded on a STOE STADIP MP diffractometer in Debye-Scherrer geometry, using Cu-$K\alpha_1$ radiation [Ge(111) Johann-type monochromator]. A sieved powdered sample (<20 μm) of LT-BeAu was diluted with quartz powder and packed under argon in a quartz capillary with a 0.3 mm diameter. A diffraction pattern was first recorded at room temperature. The graphite furnace containing the capillary was then heated to 650 °C, after which the high-temperature diffraction pattern was collected. The temperature of the graphite furnace was adjusted by determining the temperature-dependent lattice parameter of a silicon standard. Indexing of the powder pattern, structure solution, and refinement were performed with the WINCSD program package [47]. The lattice parameters for both modifications of BeAu were determined by a least-squares refinement on the peak positions.

All thermodynamic and transport measurements were performed on the annealed specimens. Temperature- and field-dependent dc magnetization measurements were carried out in a Quantum Design (QD) Magnetic Property Measurement System (XL 7) for temperatures between 2 and 300 K, and for applied magnetic fields up to $H = 0.05$ T. Magnetization data measured on arc-melted chunks and ground up powder were identical. Heat capacity was measured from 0.4 to 5 K,

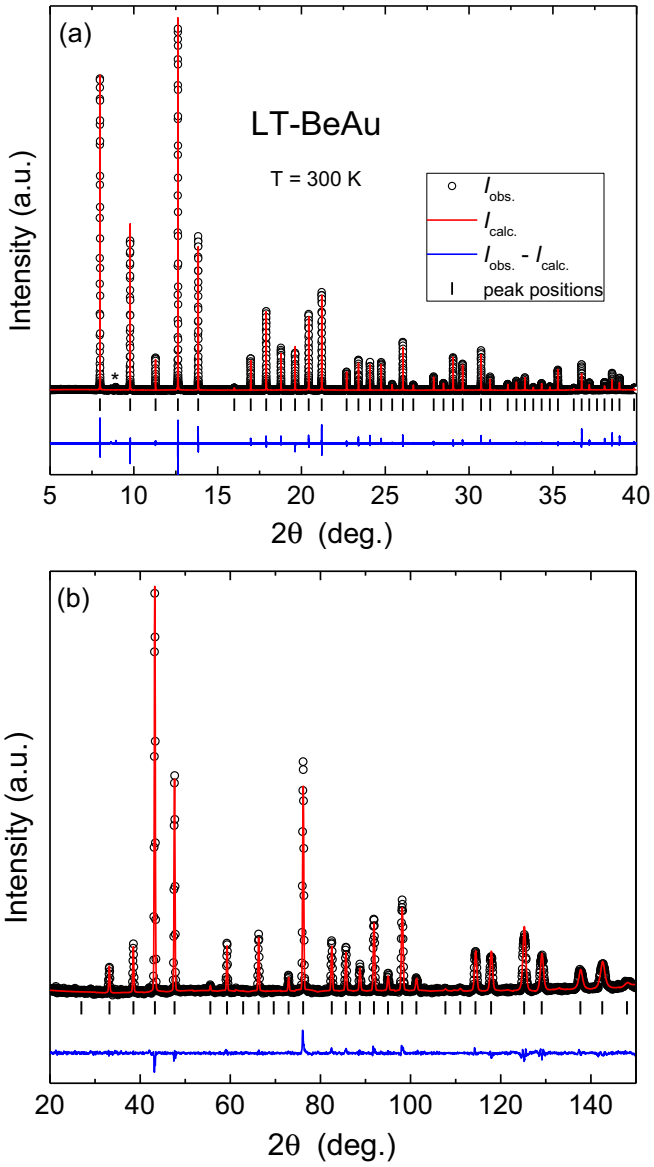

FIG. 1. (a) Synchrotron x-ray and (b) neutron powder diffraction patterns for LT-BeAu. Experimental intensities (I_{obs}) are represented by black circles, while calculated (I_{calc}) and difference intensities ($I_{obs} - I_{calc}$) are shown as red and blue lines, respectively. The black tick marks represent peak positions. Minute amounts of a secondary phase are marked by asterisks.

in magnetic fields up to $H = 0.05$ T, using a QD Physical Property Measurement System (PPMS 9, ACT option). The ac resistivity measurements in a temperature range from 1.8 to 300 K were carried out using the standard four-probe method in the QD PPMS in fields up to $H = 0.05$ T, with excitation current $i = 4$ mA and $f = 17.77$ Hz. Platinum wires were attached to the polished surfaces of bar-shaped polycrystalline sample using spot welding.

Muon spin relaxation (μSR) data were collected at the TRIUMF laboratory in Vancouver, Canada, using the LAMPF spectrometer on the M20 beamline. A helium flow cryostat was used to access temperatures between 2 and 10 K. This spectrometer gives a time resolution of 0.4 ns and achieves a

TABLE I. Crystallographic data for BeAu.

Modification	LT (FeSi type)	HT (CsCl type)
Crystal system	Cubic	Cubic
Space group	$P2_13$ (No. 198)	$Pm\bar{3}m$ (No. 221)
Pearson symbol	$cP8$	$cP2$
Formula units per cell	$Z = 4$	$Z = 1$
Molar weight	205.98 (g mol^{-1})	205.98 (g mol^{-1})
Unit-cell parameter, a	4.6699(4) Å (295 K)	2.9702(2) Å (923 K)
Unit-cell volume, V	101.844(4) Å^3	26.202(5) Å^3
Calculated density	13.37 g cm^{-3}	12.99 g cm^{-3}
	Neutron diffraction	
Wavelength, λ	1.53970 Å	
Specimen mounting	Vanadium tube	
Geometry	Transmission	
$2\theta_{min}$, $2\theta_{max}$, 2θ step	3.0°, 150.0°, 0.05°	
R_p, R_{wp}, R_{expt}, χ^2	0.0878, 0.1170, 0.1012, 1.37	
Parameters refined	4	
Weighting scheme	$w_i = Y_i^{-1/2}$	
	x-ray diffraction	
Wavelength, λ	0.459 20 Å	Cu-$K\alpha_1$; 1.540 56 Å
Specimen mounting	Quartz capillary	Quartz capillary
Geometry	Transmission	Transmission
$2\theta_{min}$, $2\theta_{max}$, 2θ step	5°, 40°, 0.001°	15°, 90°, 0.02°
R_p, R_{wp}, R_{expt}, χ^2	0.0976, 0.1315, 0.0644, 4.21	0.0495, 0.1168, 0.1138, 1.80
Parameters refined	4	2
Weighting scheme	$w_i = Y_i^{-1/2}$	$w_i = Y_i^{-1/2}$

very low background by use of a veto cup after the sample. Measurements were performed in zero field using copper electromagnets to compensate for stray fields from other instruments and the Earth's magnetic field. The field was zeroed using a fluxgate magnetometer to yield $H = 0 \pm 0.05$ G. The sample used for μSR measurements consisted of 30 slabs with thickness of ≈1 mm, covering a total area of ≈2 cm^2. The μSRFIT software package was used to fit the data. Details of the μSR technique can be found elsewhere [48–52].

Relativistic density functional theory electronic band structure calculations were performed using the full-potential FPLO code [53,54] (version fplo14.00-47). The lattice parameters and atom coordinates for LT-BeAu were taken from the neutron and x-ray diffraction data. The Perdew-Burke-Ernzerhof [55] exchange-correlation potential within the general gradient approximation was chosen. Calculations applying the local density approximation yielded essentially identical results. The spin-orbit coupling was treated nonperturbatively, solving the four-component Kohn-Sham-Dirac equation [56]. To obtain precise band structure information, the calculations were carried out on a well-converged mesh of 8000 k points (20×20×20 mesh, 700 points in the irreducible wedge of the Brillouin zone). Band structure calculations with and without spin-orbit coupling yielded essentially identical results.

III. RESULTS AND DISCUSSION

From the synchrotron x-ray powder diffraction pattern [Fig. 1(a) and Table I], the crystal structure of LT-BeAu was solved and refined in the cubic space group $P2_13$. A neutron powder diffraction experiment [Fig. 1(b) and Table I] was performed in order to precisely determine the Be position, as the coherent scattering length b_{coh} is of similar magnitude for Be [b_{coh}(Be) = 7.79(1) fm] and Au [b_{coh}(Au) = 7.63(6) fm] [57]. Confirming the previous paper [41], LT-BeAu crystallizes in the noncentrosymmetric cubic FeSi structure type with a lattice parameter $a = 4.6699(4)$ Å. This structure type can be derived from the rock-salt type by stretching the crystal structure along the trigonal axis, which, in turn, changes the octahedral coordination of atoms [Fig. 2(c)]. Au atoms are surrounded by 7 Be atoms with 2.460 Å ⩽ $d_{Be\text{-}Au}$ ⩽ 2.527 Å and 6 Au atoms with $d_{Au\text{-}Au} = 2.879$ Å (Table III). Be atoms are coordinated by 7 Au atoms with 2.460 Å ⩽ $d_{Be\text{-}Au}$ ⩽ 2.527 Å and 6 Be atoms with 2.885 Å ⩽ $d_{Be\text{-}Be}$ ⩽ 2.886 Å. Due to the similar atomic radii of Au and Be, the crystal structure of LT-BeAu geometrically does not deviate from the centrosymmetric one: since $1 - x(\text{Au}) - x(\text{Be}) = 0.0041$ here, the noncentrosymmetricity has only chemical reasons. No evidence for an extended homogeneity range of BeAu

TABLE II. Atomic coordinates and displacement parameters (in Å^2) for BeAu, obtained from powder diffraction data.

Atom	LT-BeAu					HT-BeAu				
	Site	x/a	y/b	z/c	B_{iso}	Site	x/a	y/b	z/c	B_{iso}
Au1	4a	0.1500(5)	x	x	0.64(13)	1a	0	0	0	1.1(7)
Be1	4a	0.8459(4)	x	x	0.9(2)	1b	1/2	1/2	1/2	1.8[a]

[a] B_{iso}(Be) is fixed.

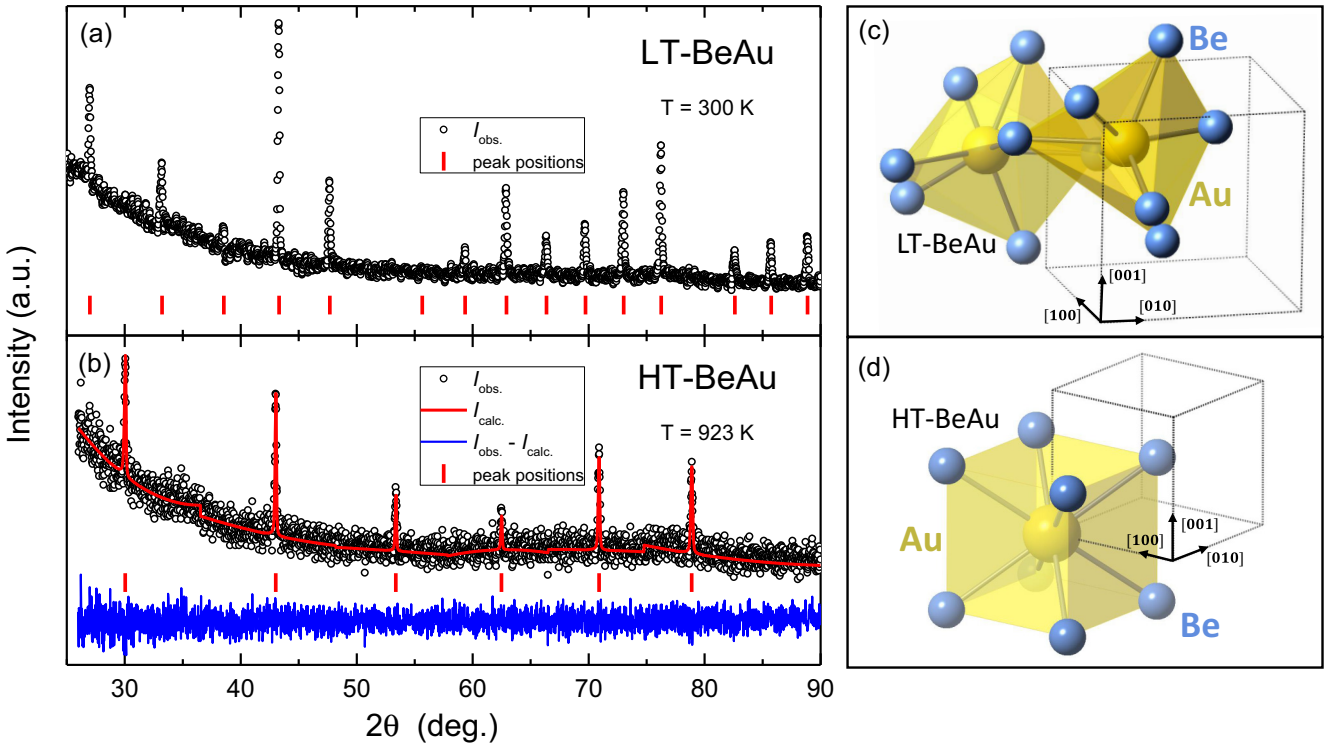

FIG. 2. X-ray powder diffraction pattern of BeAu, taken at $T = 300$ K (a) and $T = 923$ K (b). Peak positions are represented by vertical tick marks. Crystal structures of LT-BeAu (FeSi type) (c) and HT-BeAu (CsCl type) (d). Au and Be atoms are represented by large yellow and small blue spheres, respectively.

was found, as the lattice parameters change by less than one standard deviation between samples with excess of Be or Au. Therefore, the evolution of physical properties as a function of composition was not investigated.

A transition from a low-temperature FeSi type modification to a high-temperature one in the CsCl type was reported for RuSi [58]. In FeSi, the transition to the CsCl structure was induced by the application of pressure [59]. Given that the possibility of a structural phase transition in BeAu was previously suggested [43], differential thermal analysis was performed in the range from 700 to 1100 K. A strong, reversible thermal effect was observed at $T_s = 860$ K (Fig. 3), which prompted further crystallographic examination.

It was, however, not possible to quench the HT-BeAu modification to room temperature, thus, *in situ* high-temperature x-ray powder diffraction was taken at $T > T_s$. The x-ray diffraction data, collected at $T = 300$ and 923 K, are shown in Figs. 2(a) and 2(b), respectively. Atomic coordinates and displacement parameters for the two phases are summarized in Table II. The $T = 300$ K diffraction pattern is consistent with the FeSi structure type, shown in Fig. 2(c), while the $T = 923$ K data indicate a transformation into the CsCl structure type, depicted in Fig. 2(d). The crystal structure of

TABLE III. Shortest interatomic distances in LT-BeAu.

	Coordination	Distance (Å)		Coordination	Distance (Å)
Au1	1×Be1	2.459(3)	Be1	1×Au1	2.459(3)
	3×Be1	2.489(3)		3×Au1	2.489(3)
	3×Be1	2.525(3)		3×Au1	2.525(3)
	6×Au1	2.878(3)		6×Be1	2.885(2)

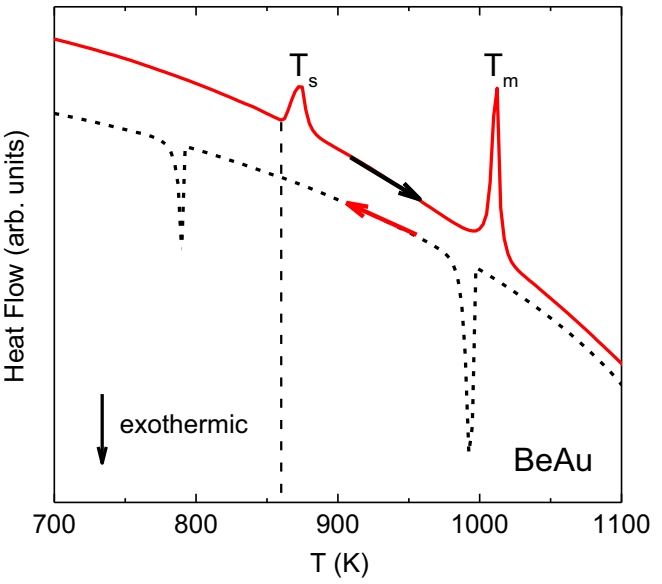

FIG. 3. Differential thermal analysis curve for BeAu taken on heating (solid red curve) and on cooling (dashed black curve). The endothermic anomaly at $T_s = 860$ K (vertical dashed line indicates the onset temperature) corresponds to the structural phase transition, while the second, larger feature marks the melting point with $T_m = 995$ K.

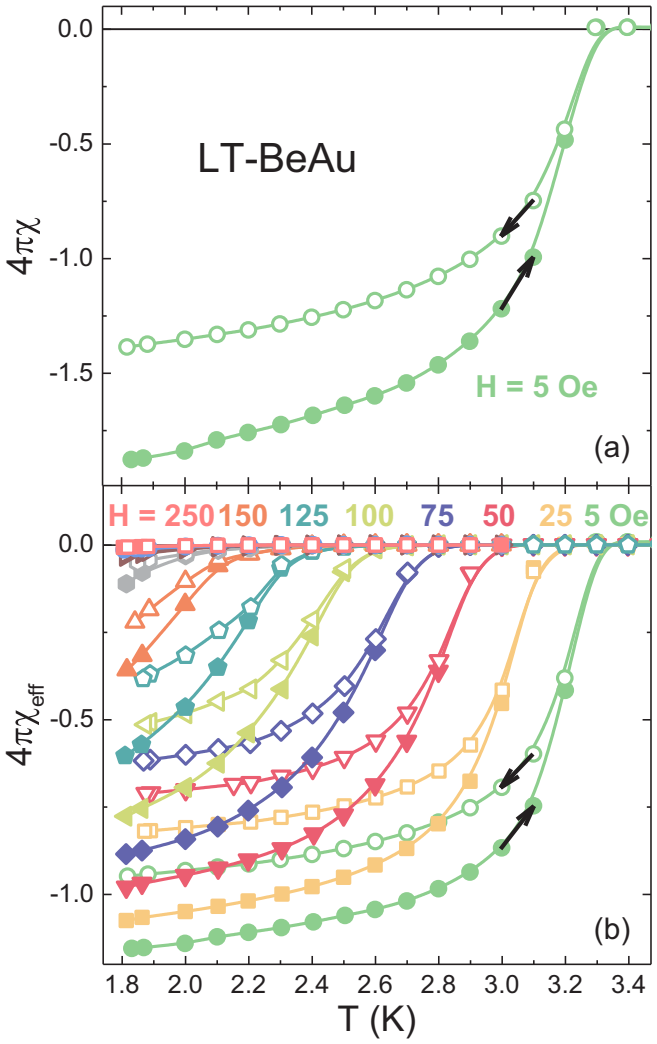

FIG. 4. (a) Zero-field-cooled (full symbols) and field-cooled (open symbols) temperature-dependent magnetic susceptibility data, scaled by 4π, for LT-BeAu in $H = 5$ Oe. (b) The temperature-dependent susceptibility data for 5 Oe $\leqslant H \leqslant$ 250 Oe were corrected for demagnetizing effects using Eq. (1). Note: 1 Oe $= (1000/4\pi)$ A/m.

HT-BeAu was refined to yield a lattice parameter $a = 2.9702(2)$ Å. In HT-BeAu, Au atoms are coordinated by eight Be atoms with $d_{\text{Be-Au}} = 2.572$ Å and six Au atoms with $d_{\text{Au-Au}} = 2.970$ Å.

The temperature-dependent magnetic susceptibility of LT-BeAu is shown in Fig. 4 for $H = 5$ Oe. Both zero-field-cooled (full symbols) and field-cooled (open symbols) data show a sharp diamagnetic transition at $T_c = 3.3$ K, demonstrating the onset of bulk superconductivity. The Meissner fraction values exceed 100%, calling for a geometric correction, using the following expression:

$$4\pi\chi_{\text{eff}} = \frac{4\pi\chi}{1 - N_d\chi}, \tag{1}$$

where $N_d = \frac{1}{3}$ is the demagnetizing factor for a spherical or cubic sample geometry [60,61]. Resultant scaled data are shown in Fig. 4(b) for 5 Oe $\leqslant H \leqslant$ 250 Oe. The application

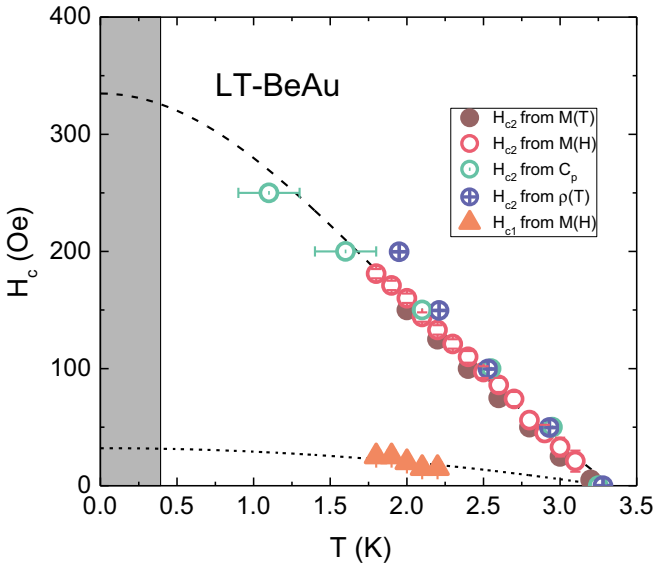

FIG. 5. (a) H-T phase diagram for LT-BeAu. The values of the critical field $H_{c1}(T)$ (triangles) are extracted from $M(T)$ data, while the values of $H_{c2}(T)$ (circles) are taken from susceptibility $M(T)$ (full), magnetization $M(H)$ (open), specific heat C_p (dotted), and resistivity $\rho(T)$ (crossed). Dotted and dashed lines are fits of the data to Eqs. (6) and (7), respectively, extrapolated to give $H_{c1}(0)$ and $H_{c2}(0)$.

of a magnetic field rapidly suppressed superconductivity, such that T_c becomes smaller than 1.8 K for $H \geqslant 175$ Oe. This allows to extract the values of the upper critical field H_{c2}, corresponding to entrance into the normal state (these values are represented with full circles in Fig. 5). Another estimate of the superconducting transition temperature $T_c(H)$ comes from the field-dependent magnetization data, shown in Fig. 6. These data were again scaled to account for the demagnetization effect. The isothermal magnetization curve for $T = 1.8$ K, shown in Fig. 6(a), was taken as a function of increasing (full symbols) and decreasing (open symbols) magnetic field. The magnetization curve is typical for a type-II superconductor [62]. The magnetic isotherms for 1.8 K $\leqslant T \leqslant$ 3.3 K, plotted in Fig. 6(b), were used to estimate H_{c1} and H_{c2}. The values of the lower critical field H_{c1} are defined as the field at which the $M(H)$ curves deviate from the line with the initial slope of the $M(H)$ curve. These values decrease monotonically with increasing temperature and are summarized in Fig. 5 as orange triangles.

Bulk superconductivity of LT-BeAu is also confirmed *via* specific-heat measurements, shown in Fig. 7: a sharp superconducting transition occurs at $T_c = 3.3$ K, in agreement with the magnetization data presented above. In the normal state, the specific-heat data are well represented by $C_p = \gamma T + \beta T^3$, in accordance with Fermi-liquid theory [62]. A linear fit to C_p/T versus T^2 above T_c (not shown) gives the value of the Sommerfeld coefficient $\gamma_n = 1.94$ mJ/mol K^2 $= 1.27\times10^2$ J/m^3 K^2 and $\beta = 66.4$ μJ/mol K^4. These values are similar to what has been reported for other NCSCs [63–67]. Using the value of γ_n, it is possible to estimate the effective mass m^* from the following relation [62]:

$$m^* = \frac{\gamma_n\hbar^2k_F^2}{\pi^2nk_B^2}, \tag{2}$$

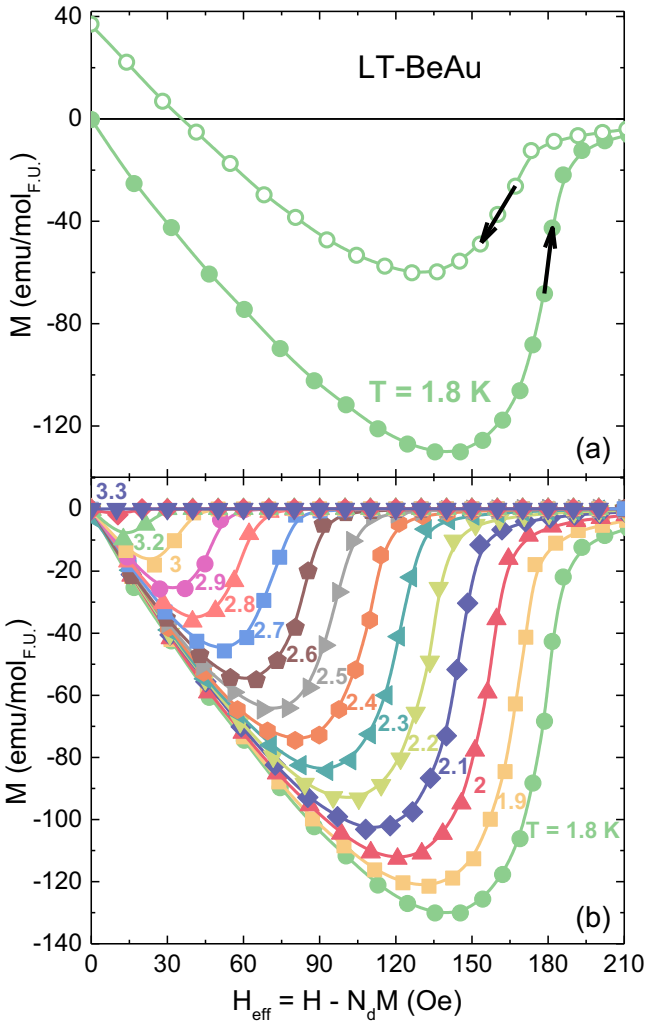

FIG. 6. (a) Field-dependent zero-field cooled (full symbols) and field-cooled (open symbols) magnetic isotherms for LT-BeAu at $T = 1.8$ K. (b) Magnetic isotherms $M(H_{\rm eff})$ for the 1.8 K $\leqslant T \leqslant$ 3.3 K temperature range. Note: 1 emu $= 10^{-3}$ A m^2.

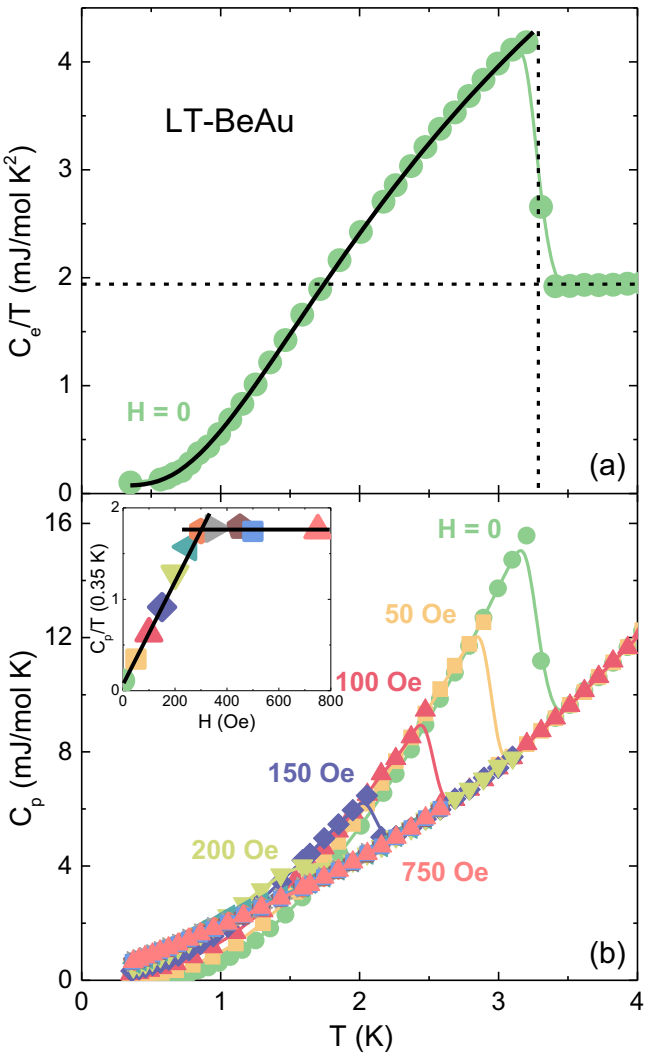

FIG. 7. (a) Electronic specific heat $C_{\rm e}$ of LT-BeAu, scaled by temperature T. The entropy conservation construction gives the ratio $\Delta C_{\rm e}/\gamma_{\rm n}T_{\rm c} \approx 1.26$ with the solid line representing a fit of $C_{\rm e}/T$ to the expected BCS relation. (b) Specific-heat data for LT-BeAu in magnetic fields $0 \leqslant H \leqslant 750$ Oe. Inset: field dependence of $\gamma_{\rm n}$, with the solid lines as guides to the eye.

where n is the charge-carrier density, calculated assuming one electron is contributed by Au, yielding $n = Z/V_{\rm cell} = 3.93\times10^{28}$ m^{-3}. The unit-cell volume $V_{\rm cell}$ is the room-temperature value, however, we expect that this quantity is only weakly temperature dependent. The Fermi wave vector $k_{\rm F}$ can then be estimated assuming a spherical Fermi surface as $k_{\rm F} = \sqrt[3]{3\pi^2 n} = 1.05$ Å^{-1}. This yields $m^* = 2.3m_{\rm e}$, indicating a nearly negligible electron mass enhancement. The value of $v_{\rm F} = 5.6\times10^5$ m/s is close to the value obtained from band structure calculations (5.1×10^5 m/s) and is comparable to what has been observed in other NCSCs [63,68,69]. Using the value of β, the Debye temperature $\theta_{\rm D}$ can be calculated from the following expression [62]:

$$\theta_{\rm D} = \sqrt[3]{\frac{14\pi^4 N_{\rm A} r k_{\rm B}}{5\beta}}, \tag{3}$$

where $r = 2$ is the number of atoms per formula unit in LT-BeAu. The value of $\theta_{\rm D} = 388$ K can then be used to estimate the strength of the electron-phonon coupling, employing the McMillan's formula [70]

$$\lambda_{\text{e-p}} = \frac{1.04 + \mu^* \ln\left(\frac{\theta_{\rm D}}{1.45T_{\rm c}}\right)}{(1 - 0.62\mu^*)\ln\left(\frac{\theta_{\rm D}}{1.45T_{\rm c}}\right) - 1.04}. \tag{4}$$

The variable μ^* represents the repulsive screened Coulomb potential with typical material-specific values in the range $0.1 \leqslant \mu^* \leqslant 0.15$. Typically, materials with $\lambda_{\text{e-p}} \to 1$ are classified as strongly coupled superconductors, while $\lambda_{\text{e-p}} \to 0.5$ indicates weak coupling [70]. For LT-BeAu, $0.48 \leqslant \lambda_{\text{e-p}} \leqslant 0.58$, which is similar to the values reported for other weakly coupled NCSCs: $LaRhSi_3$ [63], Ru_7B_3 [69], LaPtSi [66], Th_7Co_3 [68], and $Nb_{0.5}Os_{0.5}$ [33].

Once the phonon contribution to the specific heat (βT^3) has been subtracted, an equal entropy construction for the $H = 0$ data is shown in Fig. 7(a). The value for the jump in the electronic specific heat $C_{\rm e}$ at $T_{\rm c}$, $\Delta C_{\rm e}/\gamma_{\rm n}T_{\rm c} \approx 1.26$, is

comparable to the BCS value of $\Delta C_e/\gamma_n T_c = 1.44$, indicating that LT-BeAu is a weakly coupled superconductor, consistent with the $\lambda_{e\text{-}p}$ values obtained above. The superconducting electronic specific-heat coefficient γ_s can be determined as the difference between the normal-state electronic specific-heat coefficient γ_n and the residual electronic specific-heat coefficient γ_{res}. The latter can be estimated as $\gamma_{res} = C_e/T$ at the lowest temperature $T = 0.35$ K at zero field is only 0.10 mJ/mol K^2, yielding $\gamma_s = 1.84$ mJ/mol K^2. Thus, $\gamma_s \approx \gamma_n$, signifying that superconductivity of LT-BeAu is a bulk effect, consistent with the full Meissner fraction observed in magnetization (Fig. 4). The electronic specific-heat data, shown in Fig. 7(a), are fit with the expression expected from the BCS theory $C_e/T \propto e^{-\Delta/k_B T}$ [62], yielding $\Delta(0) = 0.26$ meV $= 3k_B$ K. The good agreement between the measured data (green symbols) and the BCS fit (black line) for LT-BeAu provides compelling evidence for an *s*-wave isotropic BCS superconducting gap in the electronic density of states, occurring exactly at the Fermi level. The fit yields $2\Delta(0)/k_B T_c = 3.72$, which is comparable to the weak-coupling value of 3.52, expected within the BCS theory [62]. This implies similarity of LT-BeAu with other weakly coupled NCSCs $LaRhSi_3$ (3.24 [63]), Ru_7B_3 (3.52 [69]), $Mg_{10}Ir_{19}B_{16}$ (3.59 [71]), Re_6Hf (3.64 [72]), $Nb_{0.18}Re_{0.82}$ (3.67 [73]), and Mo_3Al_2C (4.02 [74]).

Consistent with magnetization data, the application of a magnetic field suppresses T_c rapidly, as evident from the field-dependent specific-heat data, shown in Fig. 7(b). The values of H_{c2}, extracted for corresponding temperatures, are plotted in Fig. 5 as dotted circles. In order to examine the evolution of γ_n, and, hence, the nonsuperconducting density of states at the Fermi level as a function of magnetic field, $C_p/T(0.35\text{ K})(H)$ is extracted for various H. As can be seen from the inset of Fig. 7(b), a linear field dependence is followed by a plateau region. The value of $C_p/T(0.35\text{ K})(H)$ saturates above $H_{sat} = 300$ Oe $\approx H_{c2}$, consistent with what is expected for an isotropic gapped superconductor within the conventional BCS picture [62].

Another piece of evidence for the superconductivity in LT-BeAu is given by an abrupt drop in resistivity below T_c, as summarized in Fig. 8. As can be seen from the inset of Fig. 8(a), upon entering the superconducting state, $\rho(T)$ drops from ~ 1 $\mu\Omega$ cm to zero both on warming (open symbols) as well as on cooling (full symbols). The normal-state resistivity of LT-BeAu is well described within the Bloch-Grüneisen model [75–78], as evidenced by a least-squares fit [solid line in Fig. 8(a)] to the following expression:

$$\rho(T) = \rho_0 + \frac{4B}{\theta_D}\left(\frac{T}{\theta_D}\right)^n \int_0^{\theta_D/T} \frac{z^n dz}{(e^z - 1)(1 - e^{-z})} - kT^3. \quad (5)$$

The Bloch-Grüneisen relation describes the data up to room temperature, even above $\theta_D/4$, indicating significant *s*-*d* band scattering. While the value of n is typically fixed to be 2, 3, or 5 [76], the best fit for LT-BeAu is obtained for $n = 2.54$. This yields residual resistivity $\rho_0 = 0.97$ $\mu\Omega$ cm, Debye temperature $\theta_D = 398$, the electron-phonon coupling constant $B = 7.8$ mΩ cm K, and the coefficient of the cubic term $k = 3.7\times10^{-9}$ $\mu\Omega$ cm/K^3. The value of the Debye temperature θ_D is close to that extracted from the specific-heat data.

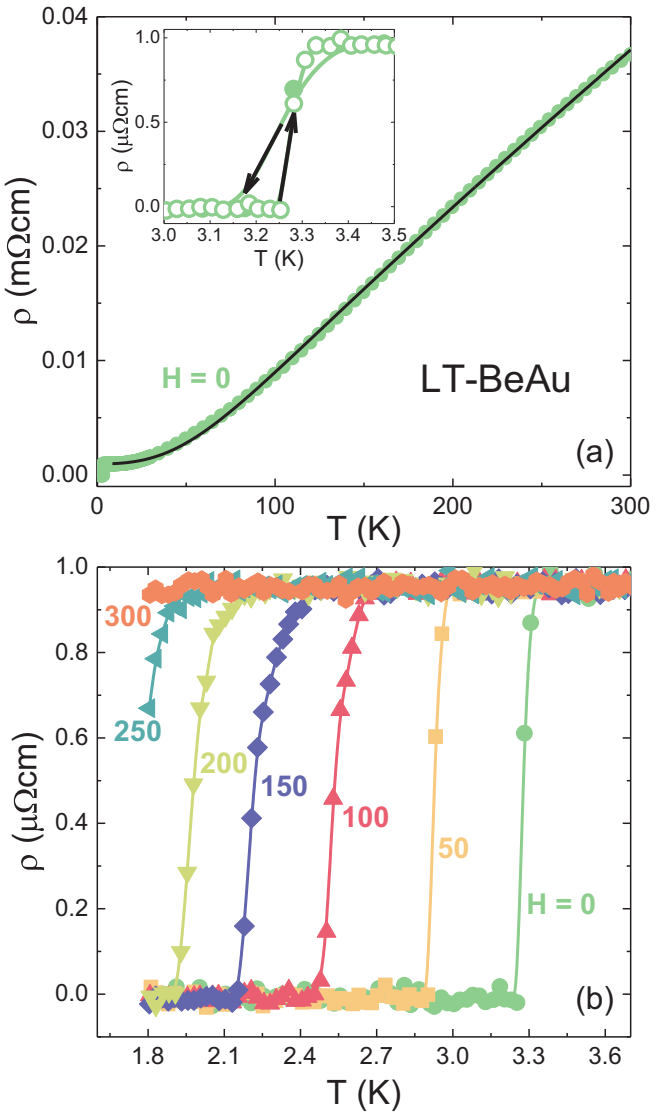

FIG. 8. (a) Zero-field temperature-dependent resistivity for LT-BeAu (green symbols), black line is a fit to the Bloch-Grüneisen expression [Eq. (5)]. Inset: data taken on warming (open symbols) and on cooling (full symbols) yields the same value of T_c. (b) Low-temperature resistivity of LT-BeAu, taken in $0 \leqslant H \leqslant 300$ Oe.

The sharp transition, the low value of the residual resistivity just above the superconducting transition, and the high residual resistivity ratio (RRR = 38), reflect good sample quality. Using the value of the residual resistivity ρ_0, Fermi velocity v_F, and the effective mass m^*, it is possible to estimate the mean-free path l within the Drude model [62]. The values of $\tau = 2.16\times10^{-13}$ s and $l = 113.7$ nm are both comparable to other NCSCs [2,63,69].

When a magnetic field is applied, as presented in Fig. 8(b), the superconducting transition is quickly suppressed. The values of $T_c(H)$, extracted from the field-dependent resistivity data using the 50% criterion, are represented in Fig. 5 as crossed circles. Together with the values obtained from magnetization and specific-heat data, they comprise the H-T phase diagram, shown in Fig. 5. First, the evolution of H_{c1} as a function of T

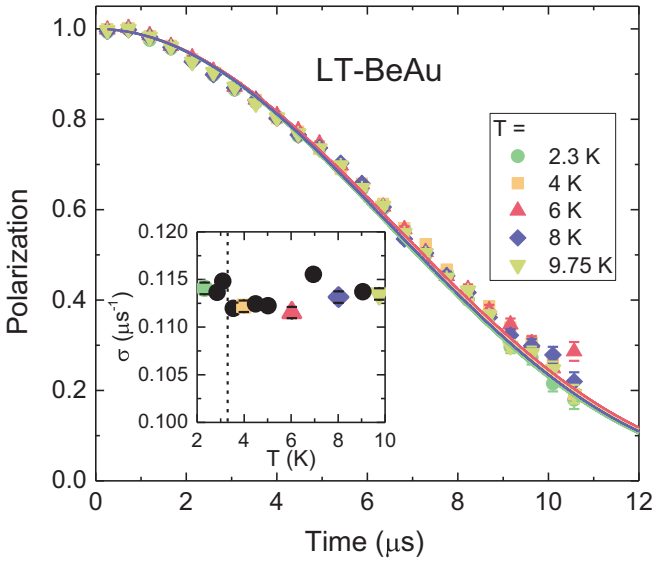

FIG. 9. Zero-field μSR data for LT-BeAu: μSR polarization spectra for 2.3 K $\leqslant T \leqslant$ 9.75 K. Symbols represent the measured data, while the solid lines are fits to Eq. (9). Inset: the relaxation rate σ, extracted from the fits to Eq. (9), does not show any temperature dependence.

is fit using the Ginzburg-Landau relation [62]

$$H_{c1}(T) = H_{c1}(0)\left[1 - \left(\frac{T}{T_c}\right)^2\right]. \quad (6)$$

The fit is shown as a black dotted line in Fig. 5, yielding $H_{c1}(0) = 32$ Oe. The evolution of the upper critical field H_{c2} as a function of temperature is shown in Fig. 5 as open and full (from magnetization data), dotted (from specific-heat data), and crossed circles (from resistivity data). Given that the influence of spin-orbit coupling for the LT-BeAu is rather weak, the data are fit with the following Ginzburg-Landau relation [62]:

$$H_{c2}(T) = H_{c2}(0)\frac{1 - \left(\frac{T}{T_c}\right)^2}{1 + \left(\frac{T}{T_c}\right)^2}. \quad (7)$$

The fit is shown as a black dashed line in Fig. 5, yielding $H_{c2}(0) = 335$ Oe. The value of $H_{c2}(0)$ can then be employed to estimate the Ginzburg-Landau coherence length $\xi_{GL}(0) = 99.1$ nm [62]. Consequently, the penetration depth is $\lambda_{GL}(0) = 231.7$ nm [79]. The Ginzburg-Landau parameter $\kappa = \lambda_{GL}(0)/\xi_{GL}(0) = 2.34 > 1/\sqrt{(2)}$, indicating that LT-BeAu is a type-II superconductor [62]. Moreover, the ratio $l/\xi_0 = 1.15$ indicates that LT-BeAu is closer to the clean limit and is consistent with the large mean-free path just above T_c. Since LT-BeAu is classified as a type-II superconductor, the thermodynamic critical field H_c was obtained using the following equation [62]:

$$H_{c1}(0)H_{c2}(0) = H_c^2 \ln[\kappa_{GL}(0) + 0.08] = 155 \text{ Oe}. \quad (8)$$

Zero-field μSR polarization spectra for LT-BeAu, collected at temperatures below and above $T_c = 3.3$ K, were examined for evidence of time-reversal symmetry breaking within the

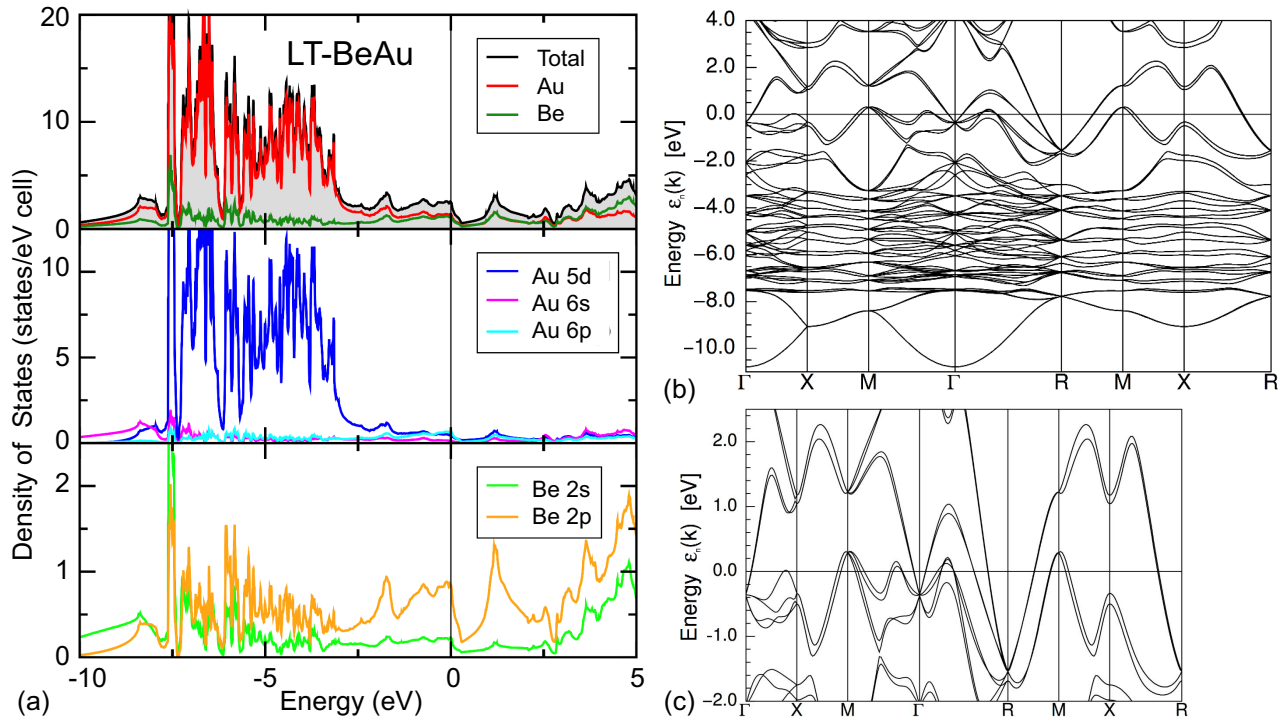

FIG. 10. Band structure calculation for LT-BeAu: (a) electronic total, partial, and orbital resolved density of states of LT-BeAu. The low-lying states are dominated by contributions of Au, whereas at the Fermi level Au and Be contribute almost equally. (b) Band dispersion of the valence band along the high-symmetry directions in LT-BeAu. The rather narrow bands in the energy window between −8 and −3 eV originate from the rather localized Au 5*d* states. The band split due to the spin-orbit coupling is moderate; at the Fermi level it is only of the order of 100 meV, as evident from (c).

superconducting state. The spectra (Fig. 9) exhibit a weakly relaxing signal, indicative of a small randomly oriented internal field in LT-BeAu. No obvious change occurs as the temperature is decreased below $T_c = 3.3$ K. The data are fit with the following equation:

$$P = \left(\tfrac{1}{3} + \tfrac{2}{3}[1 - (\sigma t)^2]e^{-\frac{(\sigma t)^2}{2}}\right), \quad (9)$$

where σ is the Gaussian relaxation rate [80]. This formula represents the static Gaussian Kubo-Toyabe function which describes the relaxation arising from a concentrated randomly oriented array of magnetic moments, consistent with what would be expected from nuclear moments. The inset of Fig. 9 shows the relaxation rate σ as a function of temperature and confirms that there is no systematic change across T_c. The scatter in σ of 0.004 μs^{-1} can be related to a change in the internal field, using the muon gyromagnetic ratio of $\gamma_\mu/2\pi = 135.5$ MHz/T as $\Delta B = \Delta\sigma/\gamma_\mu = 0.05$ G. This signals that the internal field in the sample fluctuated by 0.05 G during the measurements, which is consistent with the confidence in the zero-field condition of 0 ± 0.05 G. This suggests that no time-reversal symmetry-breaking fields exist in LT-BeAu or, at least, any such fields must have a magnitude smaller than 0.05 G. This limit is substantially smaller than the 0.08–0.5 G size of time-reversal symmetry-breaking fields that has been reported for other materials [9,37].

To gain deeper insight into the nature of the superconducting state of LT-BeAu, density functional calculations of the electronic band structure were performed, with the results summarized in Fig. 10. The states close to the Fermi energy E_F are the most relevant for superconductivity, and, as can be seen from Fig. 10(a), Au and Be bands contribute equally. The sizable contribution of Be at E_F suggests that the superconductivity is strongly related to phonon modes of the light Be atoms. Furthermore, the $5d$ and $6p$ bands of Au contribute equally, while the Be density of states is dominated by the $2p$ band. The value of the normal-state Sommerfeld coefficient γ_0, calculated using the density of states at the Fermi level $N(E_F)$, is $\gamma_0 = 1.5$ mJ/mol K^2, which is close to the experimental Sommerfeld coefficient $\gamma_n = 1.9$ mJ/mol K^2. The value of the electron-phonon coupling constant $\lambda_0 = 0.3$ is slightly less than the experimental one ($\lambda_{e\text{-}p} \to 0.5$). Away from the Fermi level, the valence band is dominated by the almost fully filled $5d$ shell of Au. The dispersion of the individual $5d$ related bands [binding energy between -8 and -3 eV, as shown in Figs. 10(b) and 10(c)] is surprisingly small, indicating a rather localized electron behavior.

IV. CONCLUSIONS

In this work, we have characterized LT-BeAu, a cubic noncentrosymmetric superconductor with $T_c = 3.3$ K. Crystallographic data along with full Meissner fraction, and a small width of the superconducting phase transition observed in magnetization, specific heat, and resistivity data, attest to the high sample purity, crystallinity, and crystallographic order. This type-II superconductor ($\kappa_{G\text{-}L} = 2.3$) is weakly coupled ($\lambda_{e\text{-}p} = 0.5$, $\Delta C_e/\gamma_n T_c \approx 1.26$) and can be well described within the BCS theory. The μSR analysis indicates that the time-reversal symmetry is preserved when the superconducting state is entered, supporting conventional superconductivity in LT-BeAu. It was also established that BeAu undergoes a structural phase transition from the low-temperature FeSi structure type modification to a high-temperature CsCl structure type at $T_s = 860$ K. Since E_F is located in a local maximum of the electronic density of states, chemical substitutions are not likely to enhance T_c. Therefore, further investigations will concentrate on the behavior of the superconducting state under application of pressure. Single crystals of both LT-BeAu and, possibly, HT-BeAu are also highly desirable and will be the focus of future work.

ACKNOWLEDGMENTS

The authors are grateful to S. Kostmann for her help during sample preparation. The identification of any commercial product or trade name does not imply endorsement or recommendation by the National Institute of Standards and Technology.

A.A. and E.S. contributed equally to this work.

[1] E. Bauer and P. Rogl, *Noncentrosymmetric Superconductors: Strong vs Weak Electronic Correlations* (Springer, Berlin, 2012).
[2] E. Bauer, G. Hilscher, H. Michor, C. Paul, E. W. Scheidt, A. Gribanov, Y. Seropegin, H. Nol, M. Sigrist, and P. Rogl, Phys. Rev. Lett. **92**, 027003 (2004).
[3] T. Takimoto and P. Thalmeier, J. Phys. Soc. Jpn. **78**, 103703 (2009).
[4] M. Shimozawa, S. Goh, R. Endo, R. Kobayashi, T. Watashige, Y. Mizukami, H. Ikeda, H. Shishido, Y. Yanase, T. Terashima *et al.*, Phys. Rev. Lett. **112**, 156404 (2014).
[5] H. Q. Yuan, D. F. Agterberg, N. Hayashi, P. Badica, D. Vandervelde, K. Togano, M. Sigrist, and M. B. Salamon, Phys. Rev. Lett. **97**, 017006 (2006).
[6] S. Chadov, X. Qi, J. Kbler, G. H. Fecher, C. Felser, and S. C. Zhang, Nat. Mater. **9**, 541 (2010).
[7] M. Z. Hasan and C. L. Kane, Rev. Mod. Phys. **82**, 3045 (2010).
[8] C. Lu and S. Yip, Phys. Rev. B **82**, 104501 (2010).
[9] G. M. Luke, Y. Fudamoto, K. M. Kojima, M. I. Larkin, J. Merrin, B. Nachumi, Y. J. Uemura, Y. Maeno, Z. Q. Mao, Y. Mori *et al.*, Nature (London) **394**, 558 (1998).
[10] J. Xia, Y. Maeno, P. T. Beyersdorf, M. M. Fejer, and A. Kapitulnik, Phys. Rev. Lett. **97**, 167002 (2006).
[11] G. M. Luke, A. Keren, L. P. Le, W. D. Wu, Y. J. Uemura, D. A. Bonn, L. Tailefer, and J. D. Garrett, Phys. Rev. Lett. **71**, 1466 (1993).
[12] P. D. de Reotier, A. Huxley, A. Yaouanc, J. Flouquet, P. Bonville, P. Imbert, P. Pari, P. C. M. Gubbens, and A. M. Mulders, Phys. Lett. A **205**, 239 (1995).
[13] M. Sigrist, Prog. Theor. Phys. **99**, 899 (1998).
[14] R. H. Heffner, J. L. Smith, J. O. Willis, P. Birrer, C. Baines, F. N. Gygax, B. Hitti, E. Lippelt, H. R. Ott, A. Schenck *et al.*, Phys. Rev. Lett. **65**, 2816 (1990).

[15] Y. Aoki, T. Tayama, T. Sakakibara, K. Kuwahara, K. Iwasa, M. Kohgi, W. Higemoto, and D. E. MacLaughlin, J. Phys. Soc. Jpn. **76**, 051006 (2007).

[16] Y. Aoki, A. Tsuchiya, T. Kanayama, S. R. Saha, H. Sugawara, H. Sato, W. Higemoto, A. Koda, K. Ohishi, K. Nishiyama *et al.*, Phys. Rev. Lett. **91**, 067003 (2003).

[17] V. G. Yarzhemsky and V. I. Nefedov, Phys. Solid State **51**, 448 (2009).

[18] A. Maisuradze, W. Schnelle, R. Khasanov, R. Gumeniuk, M. Nicklas, H. Rosner, A. Leithe-Jasper, Y. Grin, A. Amato, and P. Thalmeier, Phys. Rev. B **82**, 024524 (2010).

[19] A. D. Hillier, J. Quintanilla, B. Mazidian, J. F. Annett, and R. Cywinski, Phys. Rev. Lett. **109**, 097001 (2012).

[20] A. D. Hillier, J. Quintanilla, and R. Cywinski, Phys. Rev. Lett. **102**, 117007 (2009).

[21] A. Bhattacharyya, D. Adroja, N. Kase, A. Hillier, J. Akimitsu, and A. Strydom, Sci. Rep. **5**, 12926 (2015).

[22] A. Bhattacharyya, D. T. Adroja, J. Quintanilla, A. D. Hillier, N. Kase, A. M. Strydom, and J. Akimitsu, Phys. Rev. B **91**, 060503(R) (2015).

[23] A. A. Aczel, T. J. Williams, T. Goko, J. P. Carlo, W. Yu, Y. J. Uemura, T. Klimczuk, J. D. Thompson, R. J. Cava, and G. M. Luke, Phys. Rev. B **82**, 024520 (2010).

[24] Y. Aoki, W. Higemoto, S. Sanada, K. Ohishi, S. Saha, A. Koda, K. Nishiyama, R. Kadono, H. Sugawara, and H. Sato, Phys. B (Amsterdam) **359**, 895 (2015).

[25] E. Bauer, C. Sekine, U. Sai, P. Rogl, P. K. Biswas, and A. Amato, Phys. Rev. B **90**, 054522 (2014).

[26] B. A. Frandsen, S. C. Cheung, T. Goko, L. Liu, T. Medina, T. S. J. Munsie, G. M. Luke, P. J. Baker, M. P. Jimenez, G. Eguchi *et al.*, Phys. Rev. B **91**, 014511 (2015).

[27] W. Higemoto, A. Koda, R. Kadono, Y. Kawasaki, Y. Haga, D. Aoki, R. Settai, H. Shishido, and Y. Onuki, J. Phys. Soc. Jpn. **71**, 1023 (2002).

[28] G. Luke, M. Rovers, A. Fukaya, I. M. Gat, M. I. Larkin, A. Savici, Y. Uemura, K. Kojima, P. M. Chaikin, I. J. Lee *et al.*, Phys. B (Amsterdam) **326**, 378 (2003).

[29] G. J. MacDougall, R. J. Cava, S. J. Kim, P. L. Russo, A. T. Savici, C. R. Wiebe, A. Winkels, Y. J. Uemura, and G. Luke, Phys. B (Amsterdam) **374**, 263 (2006).

[30] G. J. MacDougall, A. A. Aczel, J. P. Carlo, T. Ito, J. Rodriguez, P. L. Russo, Y. J. Uemura, S. Wakimoto, and G. M. Luke, Phys. Rev. Lett. **101**, 017001 (2008).

[31] Z. L. Mahyari, A. Cannell, C. Gomez, S. Tezok, A. Zelati, E. V. L. de Mello, J. Q. Yan, D. G. Mandrus, and J. E. Sonier, Phys. Rev. B **89**, 020502(R) (2014).

[32] R. P. Singh, A. D. Hillier, D. Chowdhury, J. A. T. Barker, D. McK. Paul, M. R. Lees, and G. Balakrishnan, Phys. Rev. B **90**, 104504 (2014).

[33] D. Singh, J. A. T. Barker, T. Arumugam, A. D. Hillier, D. McK. Paul, and R. P. Singh, J. Phys.: Condens. Matter (2017), doi: 10.1088/1361-648X/aaa376.

[34] M. N. Wilson, A. M. Hallas, Y. Cai, S. Guo, Z. Gong, R. Sankar, F. C. Chou, Y. J. Uemura, and G. M. Luke, Phys. Rev. B **95**, 224506 (2017).

[35] Z. Zhang, Y. Xu, C. N. Kuo, X. C. Hong, M. X. Wang, P. L. Cai, J. K. Dong, C. S. Lue, and S. Y. Li, Supercond. Sci. Technol. **28**, 105008 (2015).

[36] M. A. Khan, A. B. Karki, T. Samanta, D. Browne, S. Stadler, I. Vekhter, A. Pandey, S. Teknowijoyo, K. Cho, R. Prozorov *et al.*, Phys. Rev. B **94**, 144515 (2016).

[37] R. P. Singh, A. D. Hillier, B. Mazidian, J. Quintanilla, J. F. Annett, D. McK. Paul, G. Balakrishnan, and M. R. Lees, Phys. Rev. Lett. **112**, 107002 (2014).

[38] D. Singh, J. A. T. Barker, A. Thamizhavel, D. McK. Paul, A. D. Hillier, and R. P. Singh, Phys. Rev. B **96**, 180501(R) (2017).

[39] P. K. Biswas, H. Luetkens, T. Neupert, T. Sturzer, C. Baines, G. Pascua, A. P. Schnyder, M. H. Fischer, J. Goryo, M. R. Lees *et al.*, Phys. Rev. B **87**, 180503(R) (2013).

[40] J. A. T. Barker, D. Singh, A. Thamizhavel, A. D. Hillier, M. R. Lees, G. Balakrishnan, D. McK. Paul, and R. P. Singh, Phys. Rev. Lett. **115**, 267001 (2015).

[41] B. D. Cullity, Trans. Am. Inst. Min. Metall. Eng. **171**, 396 (1947).

[42] G. P. Chatterjee, J. Mines, Metals Fuels **10**, 20 (1962).

[43] M. O. Winkler, Z. Metallkd. **30**, 162 (1938).

[44] B. T. Matthias, J. Phys. Chem. Solids **10**, 342 (1959).

[45] D. Rebar, Exploring Superconductivity in Chiral Structured AuBe, Ph.D. dissertation, Louisiana State University, 2015.

[46] A. Leithe-Jasper, H. Borrmann, and W. Hönle, in *Max Plank Institute for Chemical Physics of Solids, Scientific Report* (Dresden, 2003–2005), p. 25.

[47] L. Akselrud and Y. Grin, J. Appl. Cryst. **47**, 803 (2014).

[48] A. Schenck, *Muon Spin Rotation Spectroscopy Principles and Applications in Solid State Physics* (CRC Press, Boca Raton, FL, 1985).

[49] S. L. Lee, S. H. Kilcoyne, and R. Cywinski, *Muon Science: Muons in Physics, Chemistry and Materials* (Taylor and Francis, London, 1999).

[50] R. H. Heffner and K. Nagamine, J. Phys.: Condens. Matter **16**, 4403 (2004).

[51] A. Yaouanc and P. Dalmas de Reotier, *Muon Spin Rotation, Relaxation, and Resonance: Applications to Condensed Matter* (Oxford University Press, London, Oxford, 2010).

[52] J. E. Sonier, Muon Spin Rotation, Relaxation, Resonance, http://musr.ca/intro/musr/muSRBrochure.pdf

[53] K. Koepernik and H. Eschrig, Phys. Rev. B **59**, 1743 (1999).

[54] I. Opahle, K. Koepernik, and H. Eschrig, Phys. Rev. B **60**, 14035 (1999).

[55] J. Perdew, K. Burke, and M. Ernzerhof, Phys. Rev. Lett. **77**, 3865 (1996).

[56] H. Eschrig, M. Richter, and I. Opahle, *Relativistic Solid State Calculations in Relativistic Electronic Structure Theory (Part II, Applications)* (Elsevier, Amsterdam, 2004).

[57] V. F. Sears, Neutron News **3**, 26 (1992).

[58] L. N. Finnie, J. Less-Common Met. **4**, 24 (1963).

[59] D. P. Dobson, L. Vočadlo, and I. G. Wood, Am. Mineral. **87**, 784 (2002).

[60] J. A. Osborn, Phys. Rev. **67**, 351 (1945).

[61] A. Aharoni, J. Appl. Phys. **83**, 3432 (1998).

[62] M. Tinkham, *Introduction to Superconductivity* (McGraw-Hill, New York, 1996).

[63] V. K. Anand, A. D. Hillier, D. T. Adroja, A. M. Strydom, H. Michor, K. A. McEwen, and B. D. Rainford, Phys. Rev. B **83**, 064522 (2011).

[64] M. Isobe, H. Yoshida, K. Kimoto, M. Arai, and E. Takayama-Muromachi, Chem. Mater. **26**, 2155 (2014).

[65] B. Joshi, A. Thamizhavel, and S. Ramakrishnan, AIP Conf. Proc. **1591**, 1549 (2014).
[66] F. Kneidinger, H. Michor, A. Sidorenko, E. Bauer, I. Zeiringer, P. Rogl, C. Blaas-Schenner, D. Reith, and R. Podloucky, Phys. Rev. B **88**, 104508 (2013).
[67] S. Ramakrishnan, B. Joshi, and A. Thamizhavel, Philos. Mag. **97**, 3460 (2017).
[68] M. Sahakyan and V. H. Tran, J. Phys.: Condens. Matter **28**, 205701 (2016).
[69] L. Fang, H. Yang, X. Zhu, G. Mu, Z. Wang, L. Shan, C. Ren, and H. Wen, Phys. Rev. B **79**, 144509 (2009).
[70] W. L. McMillan, Phys. Rev. **167**, 331 (1968).
[71] T. Klimczuk, F. Ronning, V. Sidorov, R. J. Cava, and J. D. Thompson, Phys. Rev. Lett. **99**, 257004 (2007).
[72] D. Singh, A. D. Hillier, A. Thamizhavel, and R. P. Singh, Phys. Rev. B **94**, 054515 (2016).
[73] A. B. Karki, Y. M. Xiong, N. Haldolaarachchige, S. Stadler, I. Vekhter, P. W. Adams, D. P. Young, W. A. Phelan, and J. Y. Chan, Phys. Rev. B **83**, 144525 (2011).
[74] A. B. Karki, Y. M. Xiong, I. Vekhter, D. Browne, P. W. Adams, D. P. Young, K. R. Thomas, J. Y. Chan, H. Kim, and R. Prozorov, Phys. Rev. B **82**, 064512 (2010).
[75] E. Grüneisen, Ann. Phys. **16**, 530 (1933).
[76] A. Bid, A. Bora, and A. K. Raychaudhuri, Phys. Rev. B **74**, 035426 (2006).
[77] J. M. Ziman, *Electrons and Phonons* (Clarendon Press, Oxford, 1960).
[78] M. Deutsch, J. Phys. A: Math. Gen. **20**, L811 (1987).
[79] E. H. Brandt, Phys. Rev. B **68**, 054506 (2003).
[80] R. Hayano, Y. Uemura, J. Imazato, N. Nishida, T. Yamazaki, and R. Kubo, Phys. Rev. B **20**, 850 (1979).